Eur. Phys. J. B (2020) 93: 219
https://doi.org/10.1140/epjb/e2020-10295-x

THE EUROPEAN PHYSICAL JOURNAL B

Regular Article

$L2_1$ and XA ordering effect on phase stability, electronic structure, magnetic and thermodynamic properties in Scandium-Based Full-Heusler Alloys Sc_2CoZ (Z = Al, Ga, In)

Salem Hebri[1,a] and Djillali Bensaid[2,3]

[1] Ecole Normale Supérieure d'Oran, BP 1063 Saim Mohamed, Oran 31003, Algeria
[2] Department of materials sciences, Sciences institute, Belhadj Bouchaib University Center, BP 284, Ain Temouchent 46000, Algeria
[3] Laboratory of Physical Chemistry of Advanced Materials, University of Djillali Liabes, BP 89, Sidi-Bel-Abbes 22000, Algeria

Received 12 June 2020 / Received in final form 27 August 2020 / Accepted 7 October 2020
Published online 2 December 2020

Abstract. Site preference of transition metal elements habitually determined by the number of their valence electrons has been extensively used in the design of the full-Heusler alloys X2YZ. In this work, the full-Heusler materials Sc_2CoZ (Z = Al, Ga, In) were investigated and the comparison between the $L2_1$ and XA types structures of those alloys were studied based on first-principles calculations. The ferromagnetic $L2_1$ structure is found to be energetically more favorable than the XA structure. The phonon dispersion curve predicts that all alloys are dynamically stable in $L2_1$ structure. The influence of atomic ordering with respect to the Wyckoff sites on the phase stability, electronic structure and magnetism were also analyzed. Nearly half-metallic behavior is observed for the $L2_1$-type. However, XA-type is nonmagnetic semiconductor. For $L2_1$-type, all alloys have a weak magnetic moment at equilibrium lattice parameter, mainly attributed to the Co atom. Thermodynamic properties of both types of structure are studied using quasi-harmonic Debye model.

1 Introduction

Presently, Heusler alloys have gained a great deal of attention for their fascinating properties and possible uses in diverse engineering fields. These alloys have received interest of scientific researchers, because such compounds show novel properties that can be utilized in different applications such as spin injectors and magnetic junction tunnels [1–3]. Heusler alloys are not novel, the first one was discovered in 1903 by Fritz Heusler [4]. In 1983, de Groot et al. predicted that NiMnSb half-Heusler alloy is half-metallic [5], by means of ab-initio calculations. A remarkable movement of research has existed around these materials ever since. Thus, several theoretical and experimental works were dedicated to the study of the properties of these materials [6–10]. Many kinds of Heusler were found to be half metallic materials or spin-gapless semiconductors [11–14], which make theme good candidates for spintronic devices. Till now, only a small number of Heusler based semiconductors is reported [15]. Thus, it is therefore a good idea to look for more Heusler compounds that display semiconductor behavior to expand the Heusler family of electronic materials. Moreover, the semiconducting character of Heusler compounds implies their potential good transport properties for thermoelectric applications, and adequate doping for these Heusler compounds could improve their thermoelectric performance. Heusler materials have been reported by numerous researchers to be suitable thermoelectric materials and potential candidates in this field [16,17]. According to their chemical composition, Heusler alloys are classified into two main categories, the half-Heulser alloys with general formula XYZ and the full-Heusler alloys with formula X2YZ, where X and Y are transition metals, while Z is an sp element. Full Heusler alloys conventionally crystallize in two structural types, $L2_1$ type structure and Cu_2MnAl as a prototype called regular. The second structure is XA with Hg_2CuTi as a prototype called inverse Heusler. The first one belongs to the symmetry group N° 225 ($Fm\bar{3}m$) , in which X atoms occupy the (3/4, 3/4, 3/4) and (1/4, 1/4, 1/4) sites, whereas the Y and Z atoms are placed at the (1/2, 1/2, 1/2) and (0, 0, 0) sites in Wyckoff positions, respectively. In the case of XA structure with space group N° 216 ($F\bar{4}3m$), X atoms occupy the positions (3/4, 3/4, 3/4) and (1/2, 1/2, 1/2),

[a] e-mail: salem.hebri@gmail.com

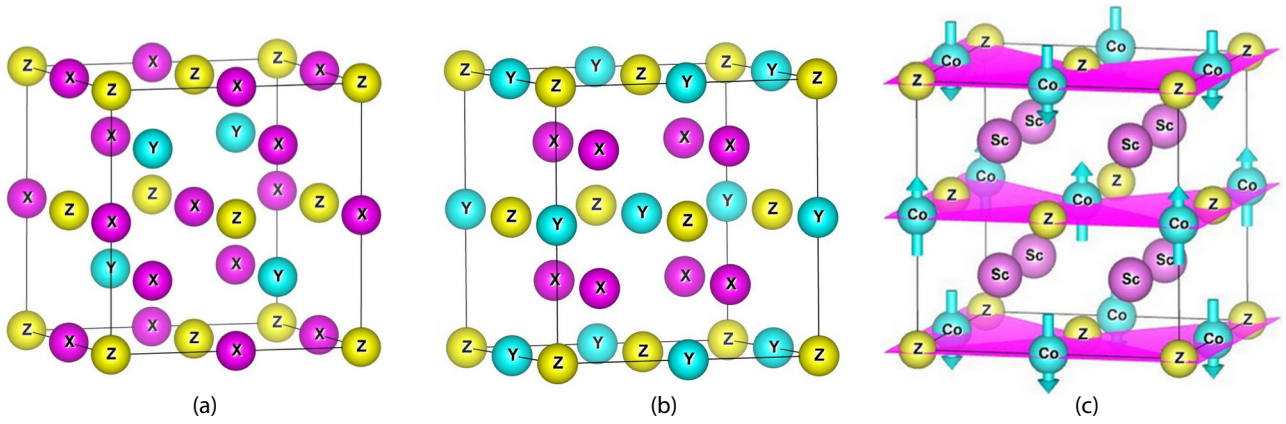

Fig. 1. Schematic representation of full-Heusler (a) XA structure with atomic sites X1 (0.75, 0.75, 0.75), X2 (0.5, 0.5, 0.5), Y (0.25, 0.25, 0.25), and Z (0, 0 , 0), (b) $L2_1$ structure with atomic sites X1 the (0.75, 0.75, 0.75), X2 (0.25, 0.25, 0.25) , Y (0.5, 0.5, 0,5), and Z (0, 0, 0), (c) the arrangement of Co magnetic moments for antiferromagnetic (AFM) configuration.

Y and Z atoms occupy the positions (1/4, 1/4, 1/4) and (0, 0, 0), respectively. According to the traditional Site Preference Rule (SPR) [18–21], the XA type structure is obtained when X element is more electronegative than Y, otherwise, the alloys crystallize in the $L2_1$ structure. However, some counter studies, including Sc_2VGe and Hf_2VZ (Z = Al, Ga, In, Tl, Si, Ge, Sn, Pb) alloys [22,23], have been pointed out recently, in which the $L2_1$-type structure is energetically the most suitable, indicating that the SPR may not be favorable for all full Heusler alloys.

In this work, we systematically studied the phase stability of Sc_2CoZ (Z = Al, Ga, In) alloys under two cubic symmetries: $L2_1$ (SG: $Fm\bar{3}m$) and XA (SG: $F\bar{4}3m$), the two structures are shown in Figure 1. We also have investigated the impact of the atomic ordering on the electronic and thermodynamic properties. This paper is ordered as follows. In next section, model and computational method are described. In the third section, results and discussion are explained. Finally, the conclusion of this study is presented in the last section.

2 Computational method

The electronic and magnetic properties of the Full Heusler Sc_2CoZ (Z = Al, Ga, In) were investigated by means of Wien2k computer package [24], based on the full-potential linearized augmented plane wave method (FPLAPW) in the frame work of the density functional theory (DFT) [25]. For structural optimization, the exchange-correlation effects were described with the Perdew–Burke–Ernzerhof parameterized generalized gradient approximation (GGA-PBE) [26]. The Brillouin zone K point integration is performed with a $17 \times 17 \times 17$ grid size for both $L2_1$ and XA structures , using the tetrahedron method. The maximum value of angular momentum $l_{\max} = 10$ is chosen for the wave function expansion within the muffin-tin spheres. The plane-wave cutoff is determined by $R_{\mathrm{MT}}k_{\max} = 8$ (where R_{MT} is the smallest muffin-in radius and $K_{\max}$ is the cutoff for the plane wave). The magnitude of largest vector used in the charge density Fourier expansion is $G_{\max} = 12$ (a.u)$^{-1}$. The electronic configurations considered for Sc_2CoZ (Z = Al, Ga, In): Sc: [Kr] $4s^2 3d^1$, Co: [Ar] $4s^2 3d^7$, Al[Ne] $3s^2\ 3p^1$, Ga: [Ar]$3d^{10}4s^2 4p^1$, In[Kr] $4d^{10}5s^2 5p^1$.

3 Results and discussion

3.1 Structural properties and dynamic properties

The atom ordering in Heusler alloys can strongly affect their properties, Consequently, in order to determine the stable ground state and obtain the equilibrium lattice constant, we investigated the site preference of Sc and Co in Sc_2CoZ (Z = Al, Ga, In) and compared the phase stability of XA and $L2_1$ structures in nonmagnetic, antiferromagnetic and ferromagnetic phases.

To achieve the antiferromagnetic (AFM) configuration, the ferromagnetic planes of Co spins (up/down) are alternatively arranged in a specific direction [001] as shown is Figure 1c, the Sc and Z atoms have zero spin polarization, since their magnetic moment contribution are insignificant as presented in Table 2.

Figure 2 shows the variation of total energy as a function of unit cell volume for both XA-type and $L2_1$-type structure in non-magnetic (NM), ferromagnetic (FM) and antiferromagnetic (AFM) cases for full-Heusler (Z = Al, Ga, In) alloys. The structural optimization curves were fitted using Murnaghan's equation of state. The ground state parameters such as optimized lattice constant a_0, bulk modulus B and its pressure derivative B' are shown in Table 1. It is clearly shown that the ferromagnetic state of $L2_1$-type structure is energetically more suitable than the XA-type structure due to its lower total energy, which is in good agreement with the work done by Han et al. [22]. For XA type structure, all curves coincide in some points, and for the other points the difference is tiny. Moreover, from Table 2 we can see that the total magnetic moments of these alloys is zero, indicating the nonmagnetic nature of these alloys in XA-type structure. It is obvious that the Z element does not affect the stability structure but the atom ordering. Many works have emphasized that Heusler alloys X_2YZ with XA-type structure

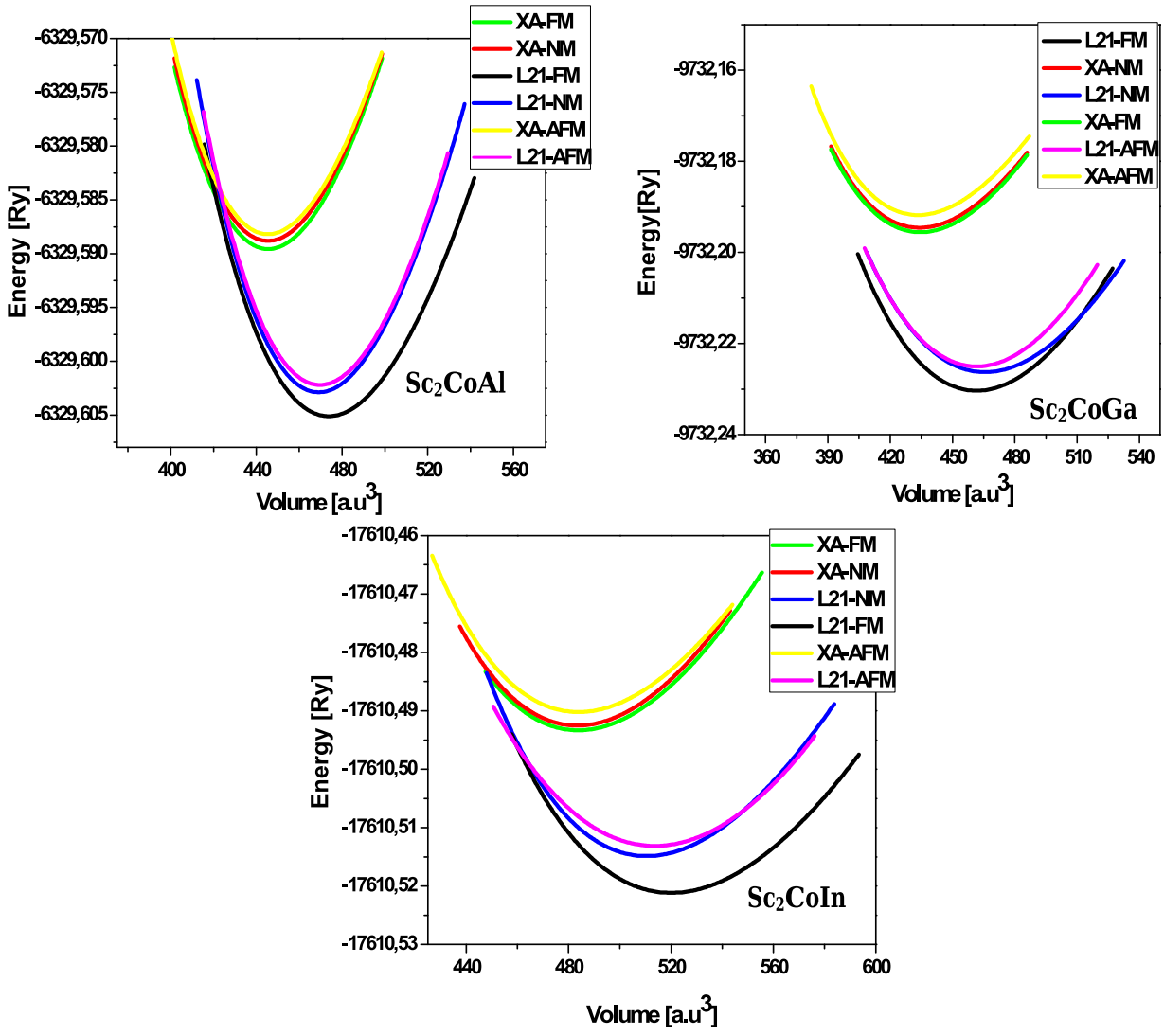

Fig. 2. The calculated total energy as a function of unit cell volume for Sc_2CoZ (Z=Al, Ga, In) with $L2_1$ and XA structures.

Table 1. Optimized lattice constant a_0 (in Å), bulk modulus B (in GPa), the pressure derivatives of the bulk modulus B', the total energy E_0 (in eV) and formation energy ΔH (in Ryd) for full Heusler Sc_2CoZ (Z = Al, Ga, In).

Alloys	Structure	a_0 (Å)	B (GPa)	B'	Emin (Ry)	ΔH (Ryd)	Stable structure
Sc_2CoAl	XA-NM	6.4151	98.28	4.4151	−6329.588763	–	
	XA-FM	6.4138	97.6809	4.6498	−6329.588844	−1.4014	$L2_1$-FM
	XA-AFM	6.4146	98.0913	4.2334	−6329.588165		
	$L2_1$-NM	6.5270	97.8257	4.0075	−6329.602880	–	
	$L2_1$-FM	6.5480	83.3271	4.0518	−6329.605104	−1.4185	
	$L2_1$-AFM	6.5294	98.8268	3.9396	−6329.602274		
Sc_2CoGa	XA-NM	6.3613	100.85	4.6853	−9732.189178	–	
	XA-FM	6.3627	100.0914	4.2232	−9732.194519	−1.4230	$L2_1$-FM
	XA-AFM	6.3611	102.4874	4.6442	−9732.191784		
	$L2_1$-NM	6.510	90.95	3.51	−9732.226274	–	
	$L2_1$-FM	6.4918	99.6263	3.3725	−9732.230352	−1.473	
	$L2_1$-AFM	6.4924	103.648	4.1680	−9732.225113		
Sc_2CoIn	XA-NM	6.5990	94.0815	3.8389	−17610.496938	–	
	XA-FM	6.5986	91.3670	3.8350	−17610.498326	−1.329	$L2_1$-FM
	XA-AFM	6.5988	91.0258	4.4582	−17610.490218		
	$L2_1$-NM	6.7132	92.9632	4.7436	−17610.514862	–	
	$L2_1$-FM	6.7553	84.5690	4.3210	−17610.521160	−1.367	
	$L2_1$-AFM	6.7303	89.6453	4.2067	−17610.513153		

Table 2. Band gaps ΔE_{gap} (eV) for Sc_2CoZ (Z = Al, Ga, In) in XA-type under the equilibrium lattice constant.

Alloys	$\Delta E_{gap}(eV)$	Other works[15]
Sc_2CoAl	0,547 (Γ-W)	0,475
Sc_2CoGa	0,630 (Γ- L)	0,532
Sc_2CoIn	0,598 (Γ-X)	0,470

(called inverse Heusler) can be found when Y element is more electronegative than the X one, such as many Sc^{-2}, Zr^{-2}, Ti^{-2}, and Mn^{-2} based Heusler compounds [27].

In order to investigate the thermodynamic stability of Sc_2CoZ alloys in both type structures and their possibility to be synthesized experimentally, we have calculated the formation energy ΔH [28,29], which is given by the following expression.

$$\Delta H = E(X_2YZ)_{\text{tot}} - 2E\,(Sc) - E\,(Co) - E(Z)$$

where $E(X_2YZ)_{\text{tot}}$ is equilibrium total energy of unit cell of Sc_2CoZ, and E(Sc), E(Co) and E(Z) are the minimized energies per atom of pure Sc, Co and Z, in their individual bulk reference structures, respectively.

We find that for $L2_1$-type structure, the formation energies of the Sc_2CoZ (Z = Al, Ga and In) are −1.418, −1.473 and −1.367 Ryd, respectively, that affirm the stability of these alloys [30,31]. On the other hand, by comparing formation energies of XA and $L2_1$-types structure (see Tab. 1), it is verified that $L2_1$-type structure is the most stable phase. A negative formation energy indicates that the three alloys can easily be synthesized experimentally in both structures.

The stability of the $L2_1$ structure type can be proven through the theoretical phonon dispersions of Sc_2CoZ (Z = Al, Ga and In), which are plotted in Figures 3a, 3b and 3c, respectively. Phonon dispersion curves of Sc_2CoZ along the high-symmetry directions have been calculated by the PHONOPY code [32]. Since the primitive cell of these alloys contains four atoms, there are altogether twelve branches consisting of three acoustic and nine optical branches in the phonon dispersion curves. There is a gap between the acoustic and the optic phonon branches which shows that Sc_2CoAl is a phononic crystal, the opposite of the other compounds, where there is a considerable overlapping between acoustic and optical phonon modes. The mass difference between Al, Ga and In atoms is the explanation of the shift in frequency. It is clear that there are no imaginary frequencies in the phonon dispersions of all three alloys, indicating the dynamic stability of all three compounds.

3.2 Calculated electronic and magnetic behaviors of $L2_1$ and XA types Sc_2CoZ

The electronic nature of a compound can be studied from its band structure and density of states. In order to understand the effect of the site preference rule depending on electronic properties in X_2YZ alloys, we compared the band structures of both structures $L2_1$ and XA.

The spin-polarized band structures for Sc_2CoZ have been calculated by FP-LAPW method within GGA at the determined equilibrium lattice constants. The Fermi level (EF) is set to zero for the band gap measurement and coincide with top of the valence band.

Figures 4a, 4b and 4c respectively show the band structure of Sc_2CoZ (Z = Al, Ga, In) alloys along high symmetry direction. It is clear that the top of the valence band and the conduction band are in different symmetry points, making these compounds semiconductor materials with an indirect band gap. These results are in agreement with other previous theoretical works [15]. The band gaps calculated and other calculated works are given in Table 2. To the best of our knowledge, there are no experimental data for comparison about the band gap. On the other hand, it has been noticed that $L2_1$ types of these alloys have nearly half-metallic behavior. Indeed, the majority spin bands are strongly metallic, while we observe the existence of the band gap in the minority band structure, where the Fermi energy passes through the valence band. The Fermi energy could be shifted to the middle of the band gap into the spin-down channel to convert the nearly half-metallic alloys into complete half-metallic materials either by applying an appropriate pressure or by doping the alloy.

To investigate the contribution of each atom to the energy bands, we have calculated the total and atomic specific spin-polarized density of states (TDOS) and partial density of states (PDOS) at their respective optimized lattice parameters under GGA approximation. The results are given in Figure 5. The graphs verified previously obtained results. Evidently, from the figure, a semiconducting band gap can be observed in both spin-up and spin-down channels for XA-type Sc_2CoZ (Z = Al, Ga, In) alloys, which is in good agreement with those band structures listed above. The Co-3d states mainly contribute in valence region of TDOS between −4 and 0 eV with sharp peaks at −1.1 eV. In the conduction between 0.5 and 2.5 eV, an hybridization occurs between Sc1, Sc2 and Co. While in the upper region above 2.5 eV only the two X atoms contribute.

On the other hand, For $L2_1$ type atomic ordering, DOS have a big difference with XA type atomic ordering. The full Heusler alloys investigated in this work show nearly metallic behaviors without semiconducting-type band gaps at Fermi level in both spin channels. As shown in Figures 5d, 5e and 5f, the spin-up and spin-down bands are crossed by the Fermi level. Both Sc and Co contribute significantly to the majority and minority states at the Fermi level position. However, the PDOS of Sc and Co becomes dispersive and band gap disappears completely in the $L2_1$ DOS. Two obvious peaks in both channels are observed mainly due to the Co-3d states, at −1.1 eV in spin-down channel and at −1.6 in spin-up channel.

In this section, we come to discuss the magnetism and Slater-Pauling rule of XA and $L2_1$ types Sc_2CoZ (Z = Al, Ga, In) alloys. The local and the total magnetic moments in interstitial and spherical region for the two types structures of Sc_2CoZ (Z = Al, Ga, In) are calculated and described in Table 3.

For the XA-type, the total magnetic moments of these alloys obey rigorously to the Slater–Pauling rule [33].

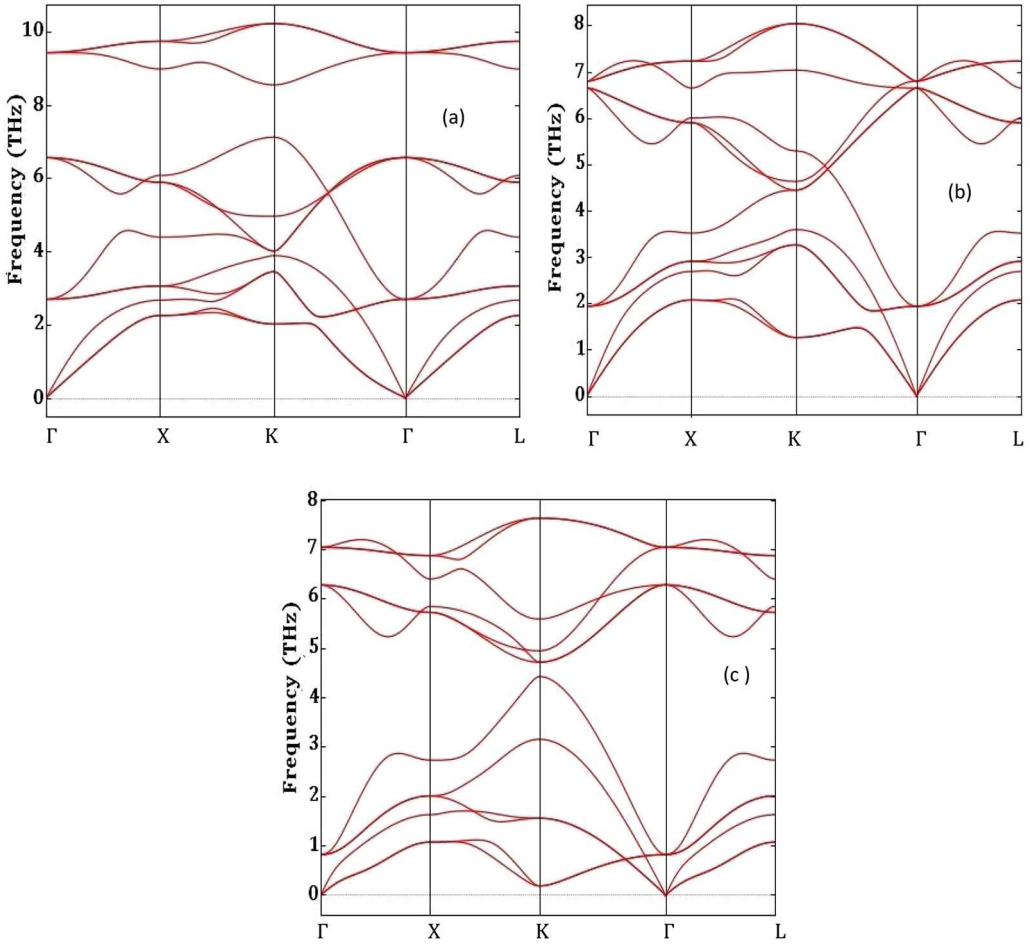

Fig. 3. The calculated phonon dispersion curves of the full Heusler compounds Sc_2CoZ at the equilibrium lattice constant. (a) Sc_2CoAl, (b) Sc_2CoGa, and (c) Sc_2CoIn.

Table 3. Calculated total and atomic magnetic moments for Sc_2CoZ (Z = Al, Ga, In) in XA-type and $L2_1$-type under the equilibrium lattice constant.

Alloys	Structure	M_{tot} (μ_β)	M_{Sc} (μ_β)	M_{Co} (μ_β)	M_Z (μ_β)
Sc_2CoAl	XA	−0.00267	Sc1 0.00654 Sc2 0.00608	−0.02080	−0.00015
	$L2_1$	0.48	−0.109	0.86393	0.00457
Sc_2CoGa	XA	−0.00013	Sc1 0.00414 Sc2 0.00011	−0.00960	0.00036
	$L2_1$	0.8	−0.11979	1.16382	0.03175
Sc_2CoIn	XA	−0.00298	Sc1 0.00555 Sc2 0.01624	−0.03819	0.00059
	$L2_1$	0.909	−0.128	1.254	0.022

Therefore, the total magnetic moment per unit cell of Full-Heusler alloys in XA type structure must follow the rule:

$$M_t = N_V - 18$$

where M_t is the total magnetic moment per unit cell and N_V is the total number of valence electrons). However, that the Slater–Pauling rule is inapplicable in the case of $L2_1$ type. That is to say, the changes in atomic occupation will lead to significant changes in their electronic and magnetic behavior. To further examine how the atomic magnetic moments change when the lattice constants is changed, we calculated the atomic magnetic moments of Sc_2CoZ (Z = Al, Ga, In) alloys with the $L2_1$-type structure. The total and individual atomic magnetic moments of $L2_1$ types Sc_2CoZ alloys as a function of lattice variation are shown in Figure 6.

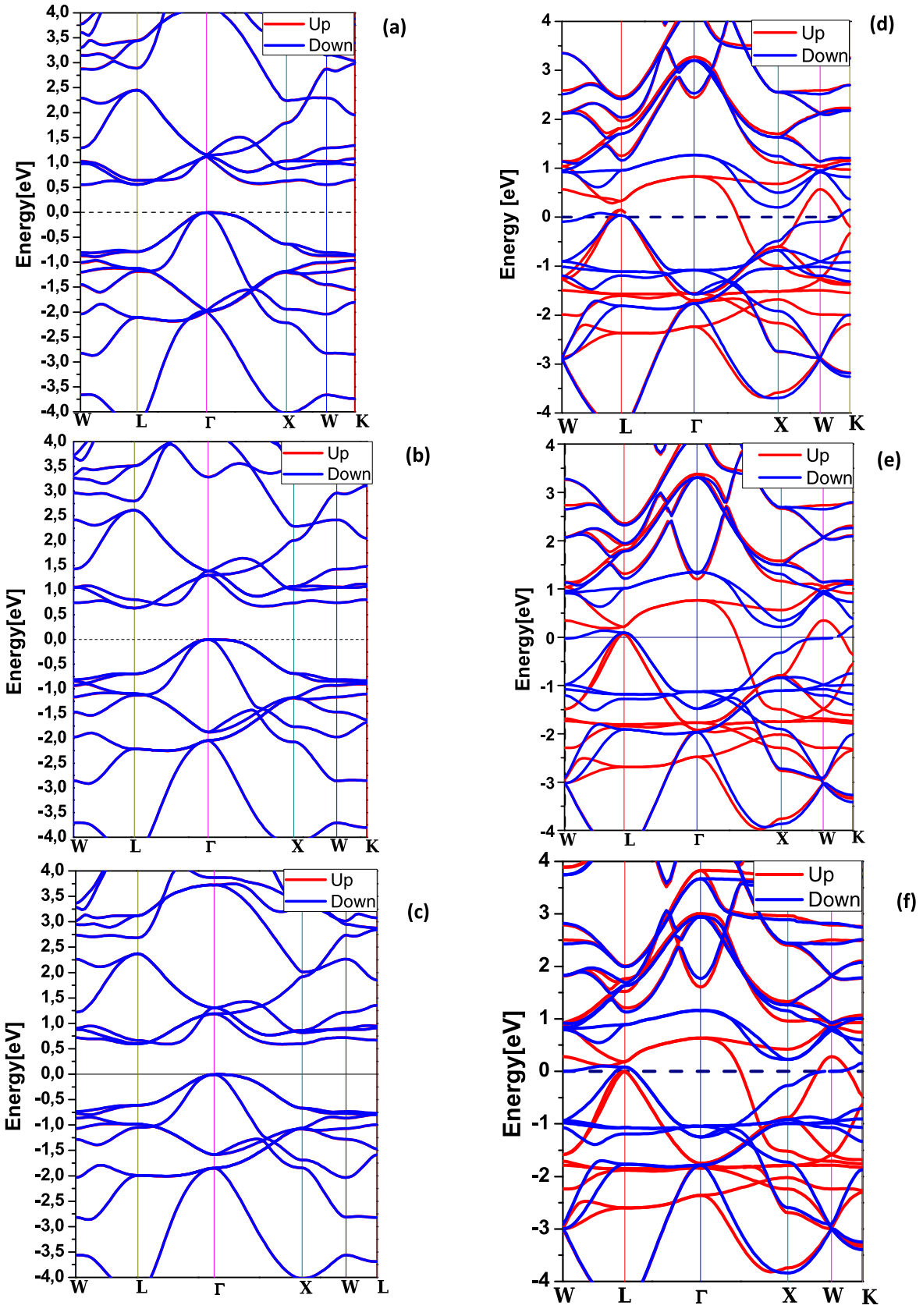

Fig. 4. Calculated band structures for Sc_2CoZ (Z = Al, Ga, In) alloys with the XA and $L2_1$ type structures at their equilibrium lattice constants: (a) Sc_2CoAl (XA), (b) Sc_2CoGa (XA), and (c) Sc_2CoIn (XA). (d) Sc_2CoAl ($L2_1$), (e) Sc_2CoGa ($L2_1$), and (f) Sc_2CoIn ($L2_1$).

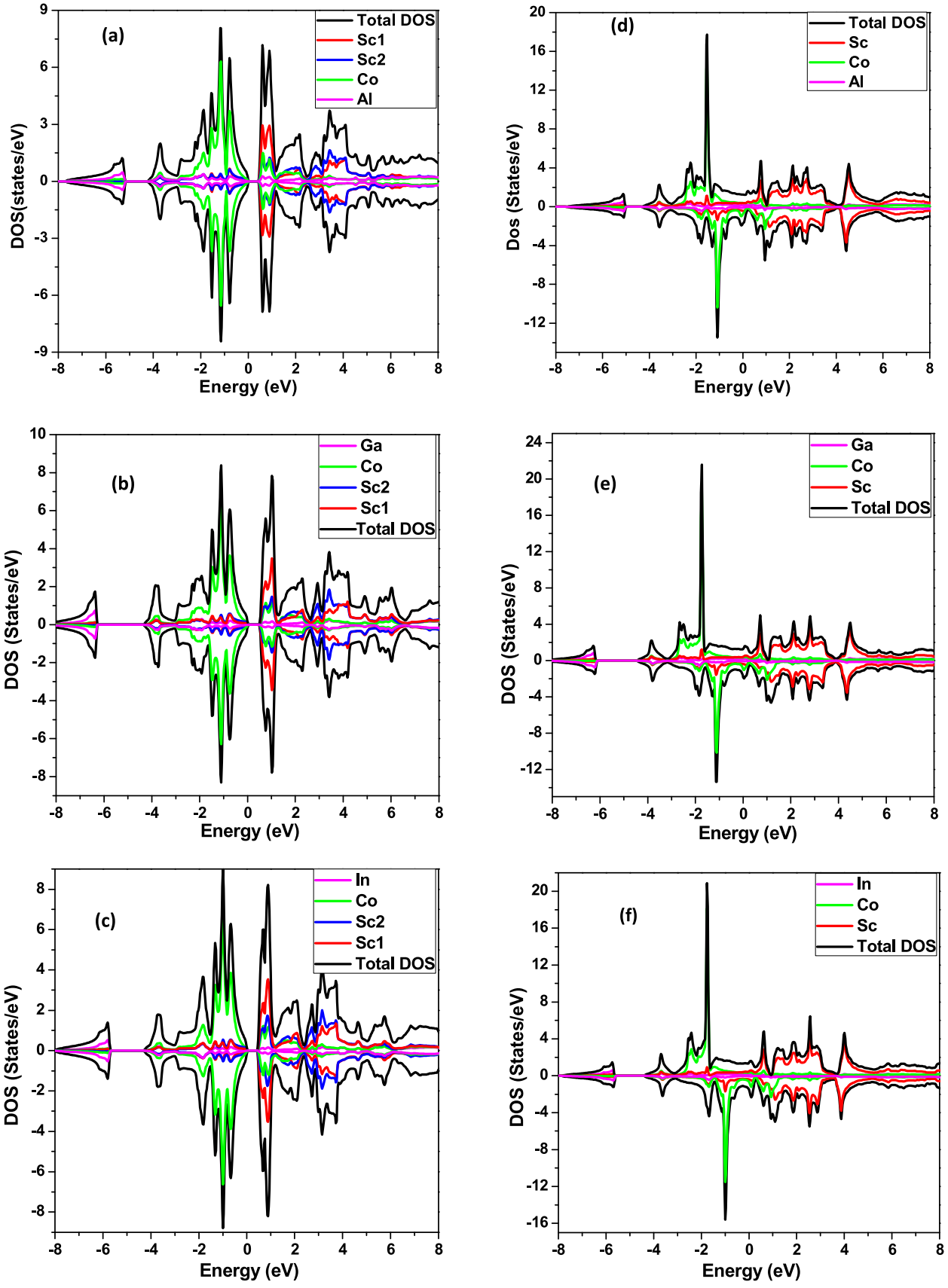

Fig. 5. Density of states (TDOS) and partial density of states (PDOS) for Sc_2CoZ (Z = Al, Ga, In) alloys with the XA and $L2_1$ type structures at their equilibrium lattice constants: (a) Sc_2CoAl (XA), (b) Sc_2CoGa (XA), and (c) Sc_2CoIn (XA). (d) Sc_2CoAl ($L2_1$), (e) Sc_2CoGa ($L2_1$), and (f) Sc_2CoIn ($L2_1$).

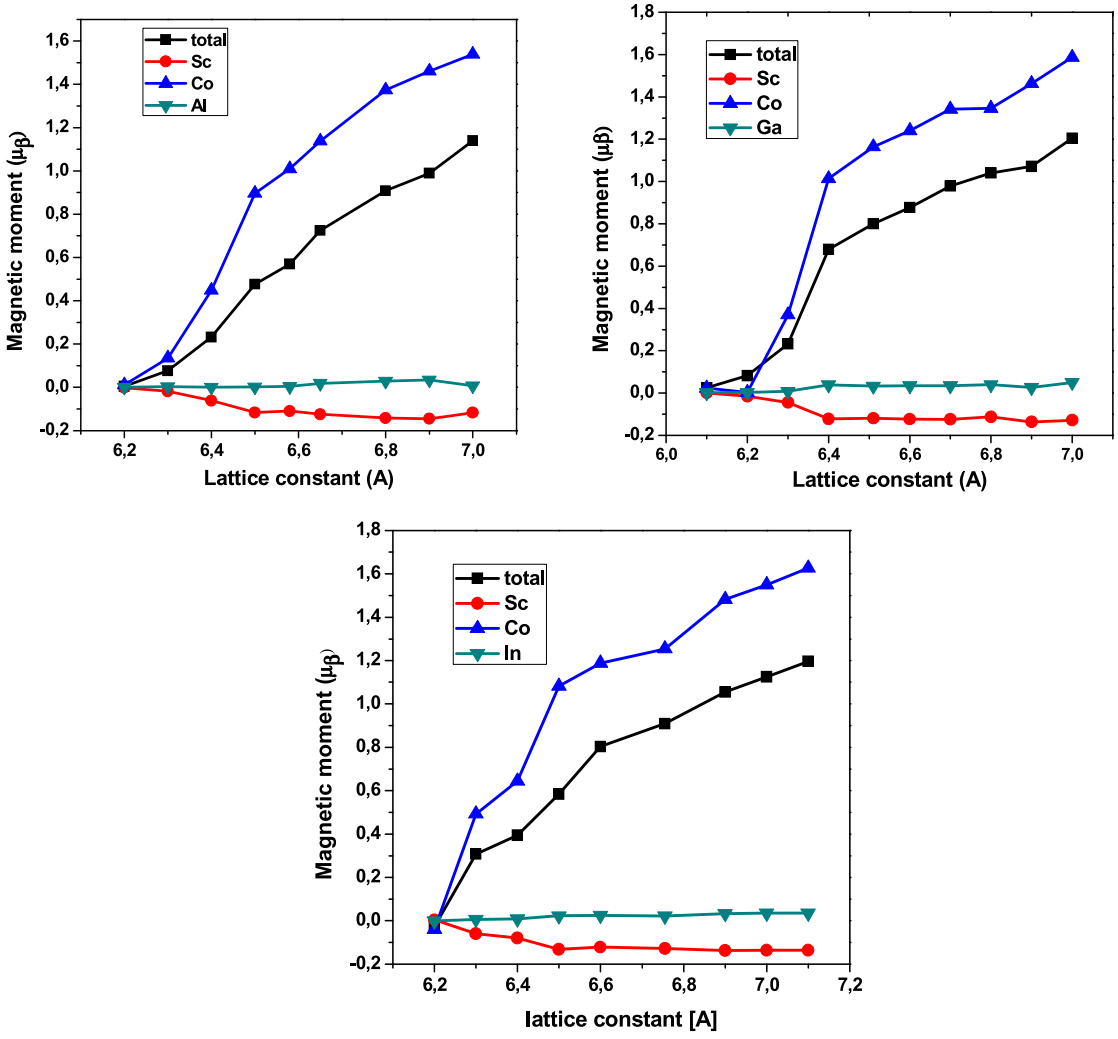

Fig. 6. Total and atomic magnetic moments as functions of the lattice constant for Sc_2CoZ (Z = Al, Ga, In) alloys with the $L2_1$-type structure: (a) Sc_2CoAl, (b) Sc_2CoGa, and (c) Sc_2CoIn.

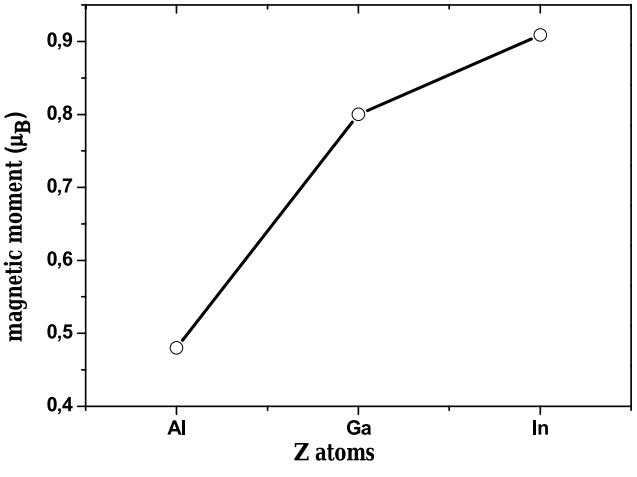

Fig. 7. Total magnetic moments versus atomic number for Sc_2CoZ (Z = Al, Ga, In) alloys with the $L2_1$-type structure.

Our calculations show that the magnetic moment of Sc_2CoZ is mostly concentrated on Co atom. With increasing lattice constant, M_t increases. Furthermore, the atomic magnetic moment of the Co atom is quite sensitive to lattice distortion. With extending the lattice constant, the atomic magnetic moment of the Co atom increases. In Figure 7, the total moments calculated for Sc_2CoZ Heusler alloys are also displayed versus atomic number. It is clear that the total moment shows a increasing trend with the rise in the atomic number.

3.3 Thermodynamic properties

Thermodynamics is necessary for materials science, device fabrications and other industrial applications. One of the important parameters is the Debye temperature, which is closely related to different physical characteristics. Quantum-mechanical effects are considered to have a significant impact on the thermodynamic properties of solids at temperatures below Debye, and may be ignored at higher temperatures [34].

The thermodynamic properties of Sc_2CoZ (X=Al, Ga, In) Heusler compounds were calculated in the

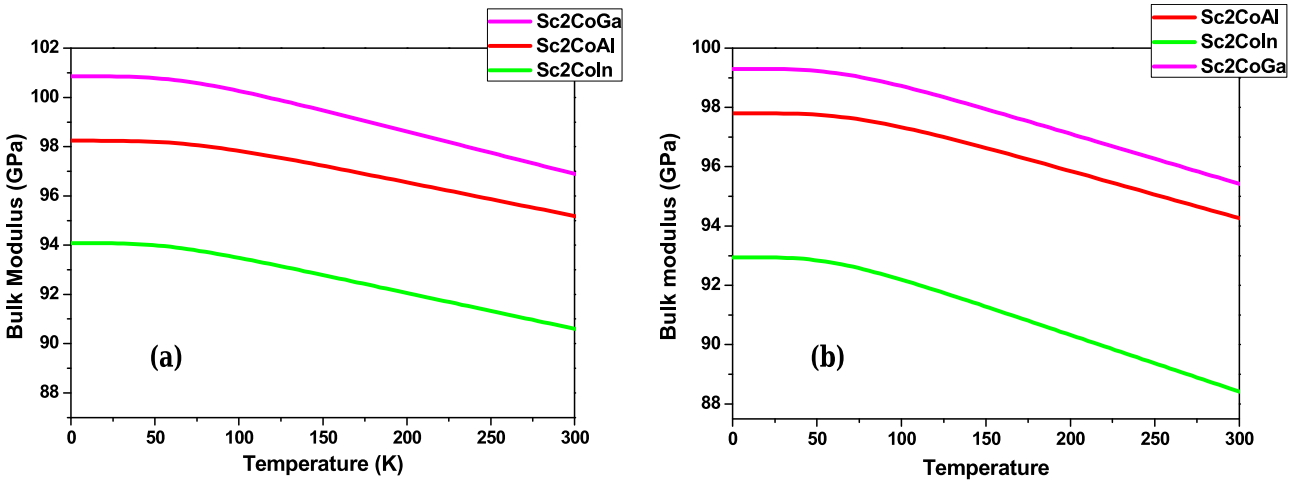

Fig. 8. The bulk modulus versus temperature: (a) XA type and (b) $L2_1$ type.

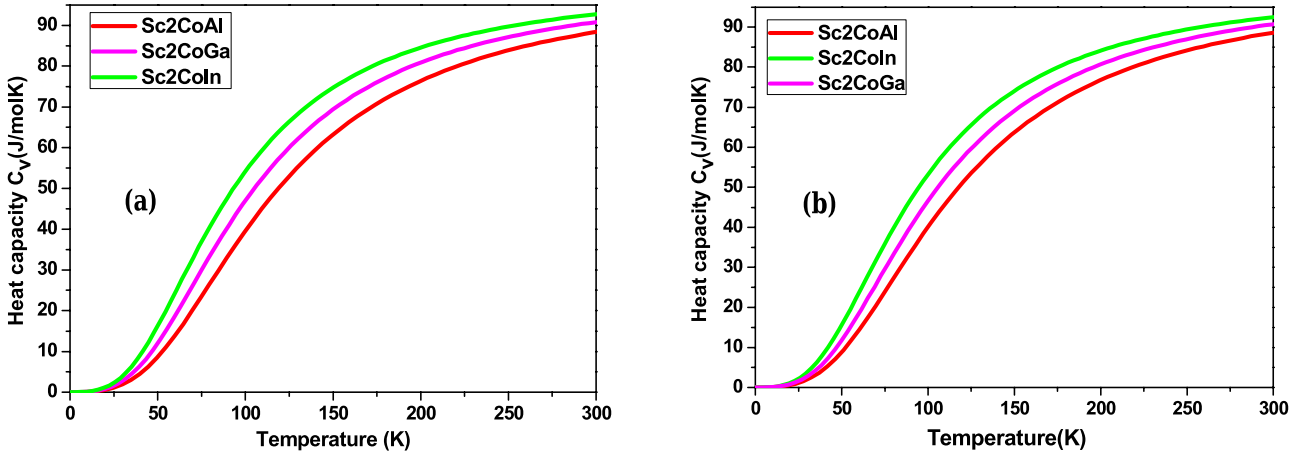

Fig. 9. The heat capacity versus temperature: (a) XA type and (b) $L2_1$ type.

temperature range of 0–300 K under zero pressure. The quasi-harmonic Debye approximation model as implemented in the GIBBS package [35] are used to estimate the bulk modulus, Debye temperature, heat capacity and thermal expansion coefficient in both structures type XA and $L2_1$.

The dependence of bulk modulus B with temperature is depicted in Figure 8. It can be shown that in these alloys the bulk modulus behaves similarly: The value of B is found to decrease with the increase in temperature for $T > 50$ K. the value of B is slightly higher in XA than $L2_1$ structure due to the change in interatomic distance.

The specific heat at constant volume C_v can provide important information, such as lattice vibration, motion of molecules and phase transition. The variation of heat capacity C_v versus temperature is plotted in Figure 9. For all alloys it could be seen that C_v increases proportionally to T_3 when $T < 150$ K and then slowly reaches the classical value of Dulong-Petit limit at higher temperature [36], which is common for all solids at high temperature due to the anharmonic effect. Furthermore, Sc_2CoIn has the biggest C_v at given pressure, which signify the ability of releasing or storing heat of Sc_2CoIn are better than the others.

Figure 10 shows the evolution of the Debye temperature θ_D versus temperature at 0 GPa. The Debye temperature is moslty used to differentiate the low- and high-temperature regions of solids. It can be seen that the Debye temperature behaves similarly to the bulk modulus. It is also shown that when $T < 50$ K, θ_D is almost invariable and with increasing temperature, Debye temperature decreases linearly with a moderate rate.

The calculations results for thermal expansion coefficient α of Sc_2CoZ Heusler alloys are presented in Figure 11. Note that the thermal expansion coefficient characterizes the variation of volume of a substance in response to a temperature change. At absolute zero temperature, coefficient α is insignificant and then it decreases with temperature in proportion to T^3, just like the heat capacity. Beyond 150 K the impact of temperature on coefficient α becomes weaker. The biggest thermal expansion coefficient was found in Sc_2CoIn for both structures. However, we should point out that the coefficient alpha is higher in XA structure type than $L2_1$ structure for all the compounds.

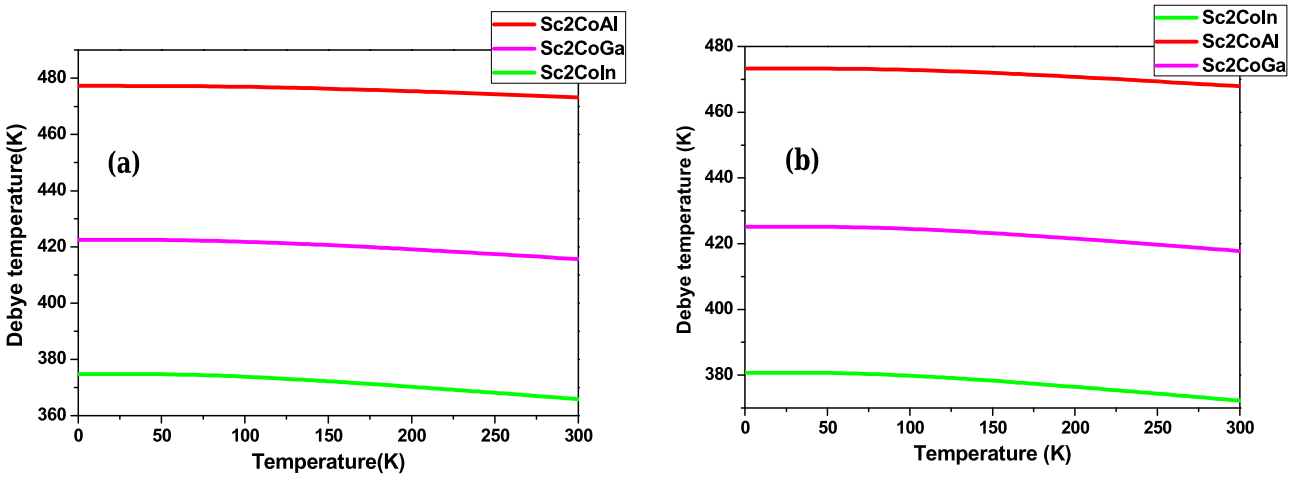

Fig. 10. The Debye temperature versus temperature: (a) XA type and (b) $L2_1$ type.

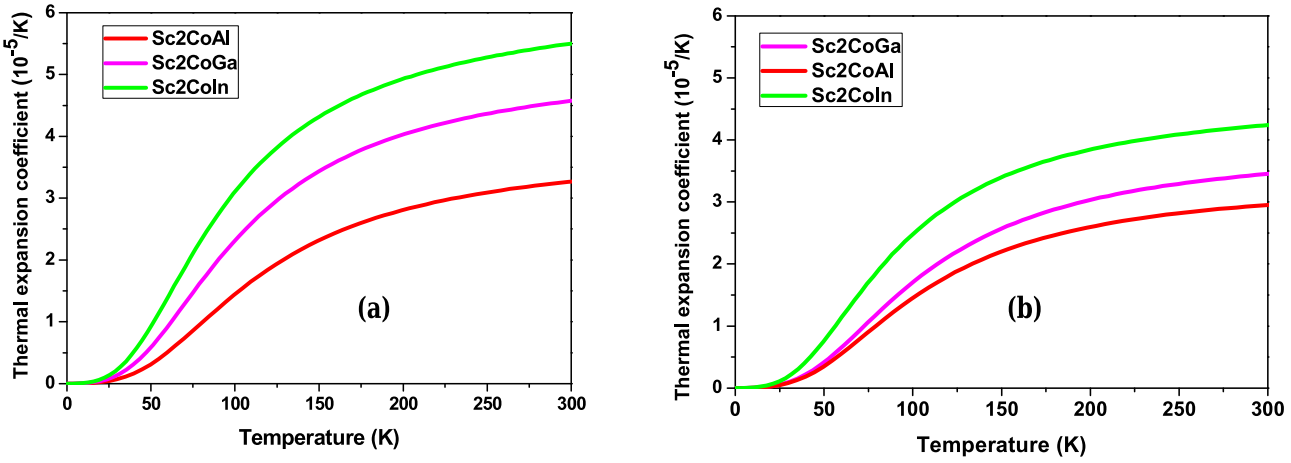

Fig. 11. The thermal expansion versus temperature: (a) XA type and (b) $L2_1$ type.

4 Conclusion

The effects of atomic site preferences on phase stability, electronic structures and magnetic properties of scandium-based full-Heusler Sc_2CoZ (Z = Al, Ga, In) have been investigated by theoretical first-principle calculations. We observed that structural, electronic and magnetic properties were affected by atomic site preferences. The results indicate that the studied compounds are energetically more favorable in $L2_1$ type structure than in XA structure.

Also, the absence of imaginary frequencies in the phonon dispersion curves confirms the dynamic stability of all three compounds in $L2_1$ type structure. The calculated electronic structures of XA-type alloys were found to be a nonmagnetic semiconductors material, which is in agreement with the Slater–Pauling theroy. However, the $L2_1$-type alloys were a magnetic metal. The lattice variation effects on magnetic moment of $L2_1$-type were also studied, and the main contribution to the total magnetism came from Co atom. That is to say, the changes in atomic occupation will lead to significant changes in their electronic and magnetic behavior. Basic thermodynamic properties, including bulk modulus, heat capacity, Debye temperature and thermal expansion coefficient expansion have been calculated as a function of temperature based on the quasi-harmonic Debye model for the XA and $L2_1$ structures. With this study, it is obvious that not all full-Heusler alloys X_2YZ obey to the site preference rule, particularly when X are low valence metal elements.

Author contribution statement

Dr Salem Hebri performed all the calculations and manuscript writing. Dr Djillali Bensaid: He proposed the idea and revised the calculations.

References

1. Enamullah, S.C. Lee, J. Alloys Compd. **765**, 1055 (2018)

2. X. Wang, Z. Cheng, H. Khachai, R. Khenata, T. Yang, J. Solid State Chem. **276**, 352 (2019)
3. Z. Chen, H. Wei, H. Xu, Y. Gao, T. Yang, X. Wang, X. Chen, Spin **3**, 1950012 (2019)
4. F. Heusler, Phys. Ges. **5**, 219 (1903) (in German). See: https://archive.org/details/verhandlungende33unkngoog
5. R.A. De Groot, FM. Muller, P.G. Van Engen, K.H.J. Buschow, Phys. Rev. Lett. **50**, 2024 (1983)
6. S. Chibani, N. Chami, O. Arbouche, K. Amara, A. Kafi, Comput. Condens. Matter **24**, e00475 (2020)
7. M.A. Hossain, Md. T. Rahman, M. Khatun, Comput. Condens. Matter **15**, 31 (2018)
8. M. Ayad, F. Belkharroubi, F.Z. Boufadi, M. Khorsi, M.K. Zoubir, M. Ameri, Y. Al-Douri, K. Bidai, D. Bensaid, Indian J. Phys. **94**, 767 (2020)
9. A. Svyazhin, E. Kurmaev, E. Shrede, S. Shamin, C.J. Sahle, J. Alloys Compd. **679**, 268 (2016)
10. N. Patra, C.L. Prajapat, P.D. Babu, S. Rai, S. Kumar, S.N. Jha, D. Bhattacharyya, J. Alloys Compd. **804**, 470 (2019)
11. S. Berri, M. Ibrir, D. Maouche, M. Attallah, Comput. Condens. Matter **1**, 26 (2014)
12. O. Cheref, F. Dahmane, S. Benalia, D. Rached, M. Mokhtari, L. Djoudi, M. Merabet, N. Bettahar, Comput. Condens. Matter **19**, e00369 (2019)
13. R. Dhakal, S. Nepal, R.B. Ray, R. Paudel, G.C. Kaphle, J. Magn. Magn. Mater. **503**, 166588 (2020)
14. M. Tas, E. Şaşıoğlu, C. Friedrich, I. Galanakis , J. Magn. Magn. Mater. **441**, 333 (2017)
15. J. Ma, J. He, D. Mazumdar, K. Munira, S. Keshavarz, T. Lovorn, C. Wolverton, A.W. Ghosh, W.H. Butler, Phys. Rev. B **98**, 094410 (2019)
16. A. Bekhti-Siad, K. Bettine, D. Prai, Y. Al-Dourid, X. Wang, R. Khenata, A. Bouhemadou, C.H. Voon, Chin. J. Phys. **56**, 870 (2018)
17. R.O. Agbaoyea, P.O. Adebamboa, B.I. Adetunjib, O. Osafilec, G.A. Adebayoa, J. Magn. Magn. Mater. **248**, 114409 (2019)
18. F. Dahmane, Y. Mogulkoc, B. Doumi, A. Tadjer, R. Khenata, S.B. Omran, D.P. Rai, G. Murtaza, D. Varshney, J. Magn. Magn. Mater. **407**, 167 (2016)
19. Y.Hu, J.M. Zhang , J. Magn. Magn. Mater. **421**, 1 (2017)
20. Z.Y. Deng, J.M. Zhang, J. Magn. Magn. Mater. **397**, 120 (2016)
21. A. Birsan, V. Kuncser, J. Magn. Magn. Mater. **406**, 282 (2016)
22. Y. Han, Z. Chen, M. Kuanga, Z. Liu, X. Wang, X. Wang, Results Phys. **12**, 435 (2019)
23. Z. Chen, H. Xu, Y. Gao, X. Wang, T. Yang, Crystals **9**, 445 (2019)
24. E. Sjöstedt, L. Nordstrm̈, D. Singh, Solid State Commun. **114**, 15 (2000)
25. P. Blaha, K. Schwarz, G.K.H. Madsen, D. Knasnicka, J. Lunitz, *WIEN2k, An augmented plane wave plus local orbitals program for calculating crystal properties* (Vienna University of Technology, Vienna, Austria, 2001)
26. J.P. Perdew, A. Ruzsinszky, G.I. Csonka, O.A. Vydrov, G.E. Scuseria, L.A. Constantin, X. Zhou, K. Burke, Phys. Rev. Lett. **100**, 136406 (2008)
27. X. Wang, Z. Cheng, R. Khenata, Y. Wu, L. Wang, G. Liu, J. Magn. Magn. Mater. **444**, 313 (2017)
28. X.T. Wang, X.F. Dai, H.Y. Jia, L.Y. Wang, X.F. Liu, Y.T. Cui, G.D. Liual, Phys. Lett. A **378**, 1662 (2014)
29. X.T. Wang, X.F. Dai, L.Y. Wang, X.F. Liu, W.H. Wang, G.H. Wu, C.C. Tang, G.D. Liu, J. Magn. Magn. Mater. **378**, 16 (2015)
30. L. Spina, Y.-Z. Jia, B. Ducourant, M. Tillard, C.Z. Belin, Kristallografiâ **218**, 740 (2003)
31. H. Nowotny, F. Holub, Monatsh. Chem. **91**, 877 (1960)
32. A. Togo, I. Tanaka, Scr. Mater. **108**, 1 (2015)
33. S.V. Faleev, Y. Ferrante, J. Jeong, M.G. Samant, B. Jones, S.S.P. Parkin, Phys. Rev. B. **95**, 045140 (2017)
34. P. Debye, Ann. Phys. **39**, 789 (1912)
35. A. Otero-de-la-Roza, D. Abbasi-Perez et al., Comput. Phys. Commun. **182**, 2232 (2011)
36. A.T. Petit, P.L. Dulong, Ann. Chim. Phys. **10**, 395 (1819)